Imparting Chemical Stability in Nanoparticulate Silver via a Conjugated Polymer Casing Approach

Mincheol Chang,[†,‡] Taejoon Kim,[⊥,‡] Hyun-Woo Park,[⊥] Minjeong Kang,[⊥] Elsa Reichmanis,*[†,§,§] and Hyeonseok Yoon*[⊥]

[†]School of Chemical and Biomolecular Engineering, [§]School of Chemistry and Biochemistry, [§]School of Materials Science and Engineering, Georgia Institute of Technology, Atlanta, Georgia 30332-0100, United States
[⊥]Alan G. MacDiarmid Energy Research Institute, Department of Polymer and Fiber System Engineering, Chonnam National University, Gwangju 500-757, South Korea

S Supporting Information

ABSTRACT: Only limited information is available on the design and synthesis of functional materials for preventing corrosion of metal nanostructures. In the nanometer regime, even noble metals are subject to chemical attack. Here, the corrosion behavior of noble metal nanoparticles coated with a conjugated polymer nanolayer was explored for the first time. Specifically, electrochemical corrosion and sulfur tarnishing behaviors were examined for Ag-polypyrrole (PPy) core−shell nanoparticles using potentiodynamic polarization and spectrophotometric analysis, respectively. First, the Ag-PPy nanoparticles exhibited enhanced resistance to electrochemically induced corrosion compared to their exposed silver counterparts. Briefly, a neutral PPy shell provided the highest protection efficiency (75.5%), followed by sulfate ion- (61.3%) and dodecylbenzenesulfonate ion- (53.6%) doped PPy shells. However, the doping of the PPy shell with chloride ion induced an adverse effect (protection efficiency, −120%). Second, upon exposure to sulfide ions, the Ag-PPy nanoparticles preserved their morphology and colloidal stability while the bare silver analog underwent significant structural deformation. To further understand the function of the PPy shell as a protection layer for the silver core, the catalytic activity of the nanostructures was also evaluated. Using the reduction of 4-nitrophenol as a representative example of a catalytic reaction, the rate constant for that reduction using the PPy encased Ag nanoparticles was found to be 1.1×10^{-3} s^{-1}, which is approximately 33% less than that determined for the parent silver. These results demonstrate that PPy can serve as both an electrical and chemical barrier for mitigating undesirable chemical degradation in corrosive environments, as well as provide a simple physical barrier to corrosive substances under appropriate conditions.

KEYWORDS: noble metals, conjugated polymers, corrosion, tarnishing, nanostructures
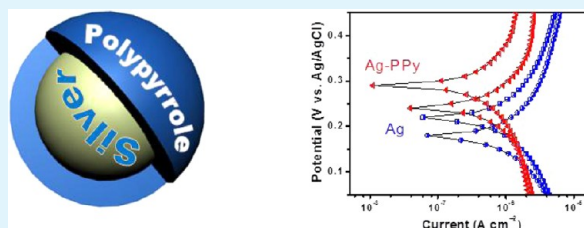
1. INTRODUCTION

Because of their superior electrical conductivity and chemical inertness in bulk states, noble metals such as gold, silver, and platinum have been utilized in a variety of applications, including chemical sensors, biotechnology, and microelectronics.[1−7] Of particular interest, they are extensively used as electrode materials in emerging all printed, flexible electronic, optoelectronic, and energy-related devices and sensor applications.[5,8−11] Although advances in lithographic technologies allow for a reduction in size of the electrodes to just a few tens of nanometers, such nanoscale structures are vulnerable to chemical and electrochemical attack during operation and also, simply upon storage in an ambient environment. Since the use of nanoscale electrodes is essential in developing state-of-the art electronics, displays, sensors, and energy devices, there is a compelling need to understand and control chemical reactivity, such as corrosion, of noble metals in the nanometer regime.

Nanometer-scale materials have unique physical and chemical properties that are not found in their bulk counterparts.[1−4] One well-known example involves the use of gold and silver nanoparticles as catalysts for chemical reactions such as C−C coupling, alkane or alkene oxidation, and the hydrogenation of dyes.[2,12] The large surface-to-volume ratio of the nanoparticles effects an increase in their chemical activity compared to the bulk materials, and thus allows them to behave as efficient catalysts. Stated in another way, in the nanometer regime, noble metals possess catalytic activities that critically depend upon their size, shape, and surface charge, in sharp contrast to the their outstanding stability at the bulk level.[2,13]

However, the enhanced surface activities obtained in the nanoregime result in such materials being prone, for instance, to corrosive deterioration, leading to critical failure in some applications, including emerging applications such as catalysis, nanophotonics, nanoelectronics, and environmental biotechnol-

ogy.[2,14−16] Noble metals can suffer from corrosion under specific conditions; For instance, silver is apt to corrode or tarnish in the presence of chloride or sulfur, and more importantly, will dissolve in aqueous solution at high applied potentials.[12−14] Thus the corrosion behavior of noble metal nanoparticles is of significant interest and some studies are beginning to emerge.[14,15] Yacaman and co-workers examined the corrosion behavior of silver nanoparticles colloidally stabilized by poly(N-vinylpyrrolidone) under atmospheric conditions,[14] and McMahon et al. demonstrated that sulfurous compounds lead to "tarnishing" of silver nanoparticles with associated significant changes in the optical characteristics of the material.[15] However, only limited information is available regarding the rational design and synthesis of functional materials having chemical, including corrosive stability in the nanometer regime.[17−19]

With the existing history of theoretical and experimental studies, most of the technical strategies for corrosion prevention and mitigation that have been devised depend upon coating or grafting of materials with protective layers such as inorganic layers, organic inhibitors, or polymers.[20−30] Notably, conjugated polymers such as polypyrrole (PPy), polythiophene, and polyaniline have been explored as protective surface coatings for metals;[23−25] such conjugated polymer coatings can provide many beneficial effects against corrosion under appropriate conditions. For instance, Fujii et al. reported the one-step synthesis of PPy-coated silver nanoparticles by dispersion polymerization and their application to an emulsifier.[31] Feng et al. also synthesized PPy-coated silver nanocomposites using an interfacial polymerization and then further functionalized the nanocomposites with gold nanoparticles for biosensor application.[32] Uniform coating of the noble metal nanoparticles with conjugated polymer layers can physically prevent interparticle aggregation and can also endow the nanoparticles with unprecedented electrical, optical, and chemical properties.[33−37]

Here, we investigate the ability of ultrathin PPy layers to protect silver nanoparticles from external chemical attack such as electrochemical corrosion and sulfur tarnishing. PPy consists of five-membered heterocyclic rings that allow π-electron delocalization along the polymer backbone. The chemical and electrical properties of PPy are based on the unique electronic structure, which can be reversibly tuned by controlling the doping state. The functional polymer, PPy was coated onto nanoparticulate silver and the ability of the conjugated polymer to protect the metal in corrosive environments was explored for the first time in the material at the nanometer scale.

2. EXPERIMENTAL SECTION

Materials. Soluble starch (ACS reagent grade), pyrrole (98%), and silver nitrate (≥99%) were purchased from Sigma-Aldrich and used without further purification. Silver nanoparticles were also obtained from Sigma-Aldrich. All other agents such as N-methylpyrrolidone (NMP), poly(vinylidene fluoride) (PVDF), sodium hydroxide (NaOH), hydrochloric acid, sulfuric acid, DBSA/isopropanol, 4-nitrophenol, poly(vinyl alcohol) (PVA, M_w = 15 000), and sodium borohydride were purchased from Sigma-Aldrich.

Synthesis of the Ag-PPy Nanoparticles. Ag-PPy core−shell nanoparticles were prepared with the careful modification of the previously reported methods.[33−39] First, 4 wt % starch was completely dissolved in 30 mL of distilled water at 260 °C. Then the starch solution was maintained at 95 °C and pyrrole monomer (75 mM) was added dropwise into the reactor. Subsequently, 250 mM silver nitrate was introduced into the above starch solution and the reaction was

allowed to proceed for 24 h at 95 °C under vigorous stirring. The Ag-PPy nanoparticles were retrieved from the resulting black colloidal solution via water washing with centrifugation, followed by vacuum drying. Ag-PPy nanoparticles with a thicker shell were synthesized under identical conditions except for a greater amount of pyrrole monomer (150 mM).

A control sample, referred to as bare silver nanoparticles was prepared by reducing silver nitrate with sodium borohydride in the presence of a steric stabilizer, poly(vinyl alcohol).[40,41] First, 1.5 g of PVA was dissolved in 50 mL of distilled water, and then 4.5 mM silver nitrate and 1.3 mM sodium borohydride were sequentially added to the PVA solution with vigorous stirring. The reaction was allowed to proceed for 4 h at 25 °C, and finally silver nanoparticles were obtained via the above purification process.

Corrosion Tests. Electrochemical measurements were carried out with a platinum counter electrode and Ag/AgCl reference electrode. The nanoparticles were mixed with 0.01 mL of PVDF/NMP (12:1 w/w) solution and then coated on 0.7 cm^2 stainless steel to use as a working electrode. The potentiodynamic polarization measurement was conducted in a miniature cell, during which water and sulfuric acid were employed as electrolytes. The cyclic polarization scan was performed from −500 to +500 mV and back to −500 mV at 500 mV s^{-1} with 10 mA as the selected current range setting. Then the potential was plotted as a function of the logarithm of the current density to produce polarization curves. Corrosion parameters such as corrosion potential, corrosion current density, Tafel slopes, and polarization resistance were derived from the Tafel extrapolation constructed using IVMAN software. Each test was repeated 5 times and the data were averaged. The protection efficiency (P) was calculated from the following equation

$$P(\%) = (I'_{corr} - I_{corr}) \times 100/I'_{corr}$$

where I'_{corr} and I_{corr} are the corrosion current densities for silver nanoparticles and the Ag-PPy nanoparticles, respectively. The value of I'_{corr} was determined from the averaged value of two silver nanoparticles. The PPy shells were dedoped by immersing the nanoparticles into 1 M NaOH solution. The PPy shells were redoped by using 1 M sulfuric acid, 1 M DBSA, and 1 M hydrochloric acid solution.

For the tarnishing test, 10 mg of the nanoparticles was mixed in 20 mL of 10 mM sodium sulfide solution for 30 min, after which the nanoparticles were separated from the solution using centrifugation. The nanoparticles were mildly rinsed with water several times and then resuspended in distilled water to take UV−visible spectra or dried in a vacuum oven at room temperature to take SEM images.

Catalysis Test. The nanoparticles were homogeneously dispersed into 100 mL of 4-nitrophenol (0.144 mM), where the concentration of silver was 0.1 wt %. The concentration of silver in solution was estimated from the absorbance of the surface plasmon resonance. Subsequently, 3 mL of the above solution was mixed with 1 mL of 1.2 M sodium borohydride solution, during which the UV−visible spectra of the reaction mixture were recorded at intervals of 60 s. The catalytic reaction proceeded at 25 °C.

Characterization. The morphology of the nanoparticles was observed by a JEOL EM-2000 EX II microscope. SEM observation was performed for the specimens with a JEOL JSM-7500F microscope. UV−visible spectra were recorded on an Agilent 8453 spectrophotometer. XPS was carried out using a Thermo VG Scientific Multilab 2000 spectrometer with an XPS Mg/Al twin-anode excitation source. Peak fitting of the collected spectra was done with VG Avantage software supplied by the manufacture. All electrochemical experiments were performed using a Wonatech WMPG 1000 potentiostat/galvanostat.

3. RESULTS AND DISCUSSION

Ag-PPy core−shell nanoparticles were obtained in the form of a stable colloidal suspension through a simple one-pot synthesis. Briefly, a silver precursor acted as an oxidizing agent for the chemical polymerization of pyrrole. The pyrrole molecules

were oxidized by silver cations, yielding PPy and silver atoms concurrently (see the scheme below).[31]
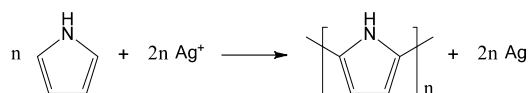
The use of an appropriate steric stabilizer (soluble starch) allowed the formation of the core−shell nanostructure.[38] Figure 1 briefly depicts the formation mechanism of Ag-PPy core−
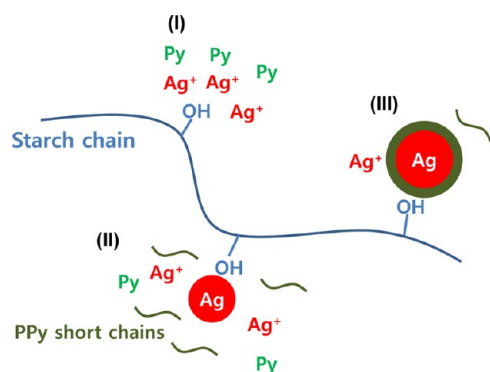
Figure 1. Schematic illustration of the formation mechanism of Ag-PPy nanoparticles: the reaction process was divided into three stages (I, II, and III).

shell nanoparticles. At the initial stage (stage I and II), the hydroxyl groups of soluble starch can act as nucleation sites where silver cations are reduced to atomic silver by the pyrrole monomers, whereas pyrrole monomers are oxidized to radical cations that lead to the generation of PPy short chains. While the silver nanoseeds are being formed at stage II, additional silver cations are adsorbed onto the nanoseed surface due to the common ion adsorption effect.[39] The silver nanoseed surfaces become the active sites for oxidation of the surrounding pyrrole monomers (or growing PPy chains) and finally to form a PPy shell (stage II and III). Bare silver nanoparticles were also employed as control samples, where one was a commercialized product and the other was prepared with careful modification of the previous method.[40,41] Figure 2 presents transmission electron microscopy (TEM) images of Ag-PPy core−shell nanoparticles and the two alternative bare silver nanoparticles. As the electron density of PPy is considerably lower than that of silver, PPy appeared brighter than silver in the TEM image. In Figure 2a, the contrast of the nanoparticles showed a darker core surrounded by a brighter shell, confirming an Ag-PPy core−shell structure. The core−shell nanoparticles exhibited relatively good colloidal stability without serious interparticle aggregation. The shell thickness was tunable by adjusting the concentration of the pyrrole monomer. Representatively, Ag-PPy nanoparticles were synthesized with an average core diameter of 36 ± 7 nm and a shell thickness of 13 ± 6 nm. The diameters of homemade (Ag-1) and commercially available (Ag-2) silver nanoparticles were 28 ± 4 and 32 ± 5 nm, respectively.

X-ray photoelectron spectroscopy (XPS) analysis was carried out to qualitatively examine the core−shell nanoparticles (Figure 3). The binding energy peaks of carbon, nitrogen, oxygen, and silver were observed in the XPS spectrum. The inclusion of Ag^0 species in the nanoparticles was confirmed by the presence of a doublet at 368.5 and 374.2 eV which
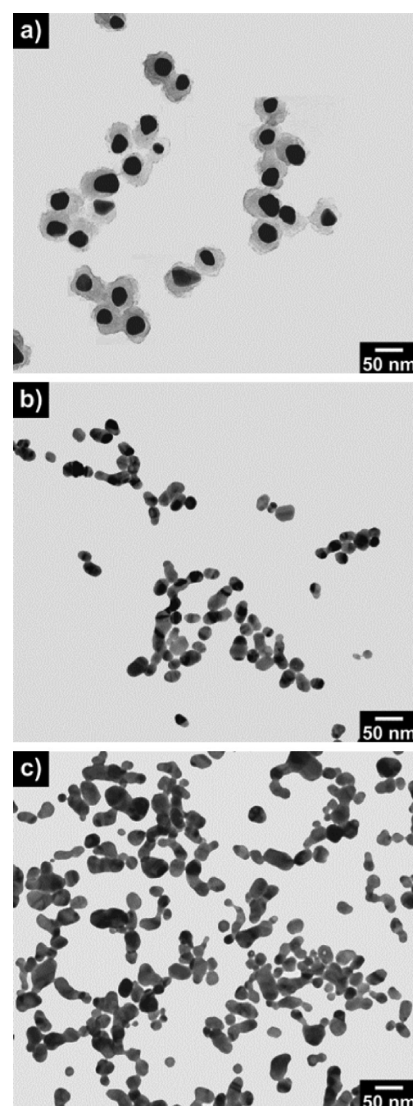

Figure 2. TEM images of (a) Ag-PPy nanoparticles, (b) Ag-1, and (c) Ag-2.

corresponds to Ag $3d_{5/2}$ and Ag $3d_{3/2}$, respectively (Figure 3a). In addition, the N 1s spectrum could be deconvoluted into three components, as shown in Figure 3b. Importantly, positively charged nitrogen (N^+) species were found at about 401 eV, indicating that the PPy forming the shell of the nanoparticles was in an oxidized state. The calculated atomic ratio of N^+ to total N species was 0.12, which corresponds to the oxidation level of the conjugated polymer: the theoretical maximum of the oxidation level is approximately 0.33. Considering the synthetic condition, only nitrate ions (NO_3^-) can act as the counterion (dopant) inside the PPy shell.

Ultraviolet (UV)-visible spectroscopy is also an effective tool to characterize the core−shell nanoparticles. The UV−visible absorption spectra of the Ag-PPy nanoparticles and control silver samples are presented in Figure 4. The one strong absorption band observed in the Ag-PPy spectrum in the vicinity of 470 nm was attributed to the surface plasmon resonance of the silver core. The surface plasmon resonance is sensitive to the surrounding environment. Compared to that of the silver nanoparticles having the same diameter,[40] the absorption profile of the Ag-PPy nanoparticles was broader

a)

Ag 3d$_{5/2}$

Ag 3d$_{3/2}$

Intensity

Binding energy (eV)

b)

N 1s

Intensity

Binding energy (eV)
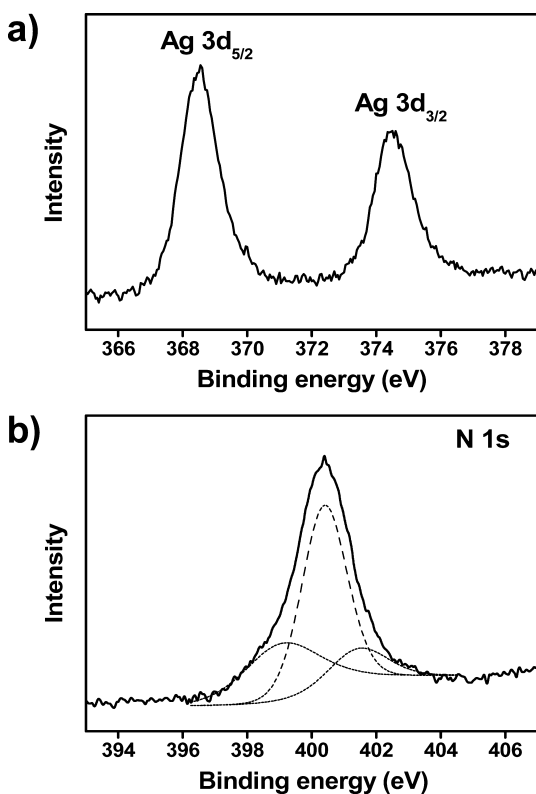
Figure 3. XPS (a) Ag 3d and (b) N 1s spectra of Ag-PPy nanoparticles: the N 1s spectrum was decomposed into three component peaks centered at 399.1, 400.4, and 401.5 eV, which were assigned to neutral imine-like (=N−), amine-like (−NH−), and positively charged (N$^+$) species, respectively.

(a)

(b)

(c)

Absorbance

Wavelength(nm)
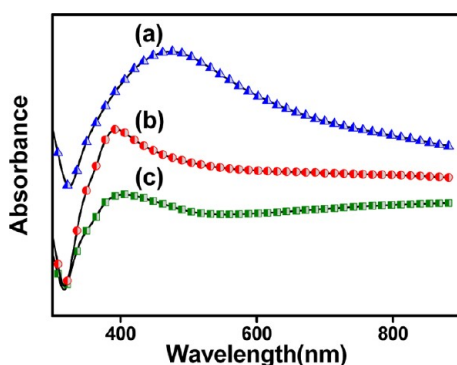
Figure 4. UV−visible spectra of (a) Ag-PPy nanoparticles, (b) Ag-1, and (c) Ag-2.

with a red-shifted feature. The control silver sample exhibited characteristic surface plasmon bands at about 400 nm. The observed change in plasmon band could be due to the surrounding PPy shell. Additionally, the PPy shell may be thin enough to allow plasmon coupling between neighboring Ag cores. Therefore, the aggregation of the core−shell nanoparticles might also contribute to the change.

As their application frequently requires immersion in solutions, noble metals often suffer from corrosion via charge transfer reactions at the metal/solution interface. Atmospheric humidity can also lead the adsorption of moisture on the metal surface, which causes troublesome atmospheric corrosion. Hence, the electrochemical corrosion behavior of the Ag-PPy nanoparticles in water was first examined using a potentiody-

namic polarization technique. Figure 5 shows the effect of PPy shell thickness on the corrosion behavior of the core−shell

Potential (V vs. Ag/AgCl)

(b)

(a)

(c)

(d)

Current (A cm^{-2})
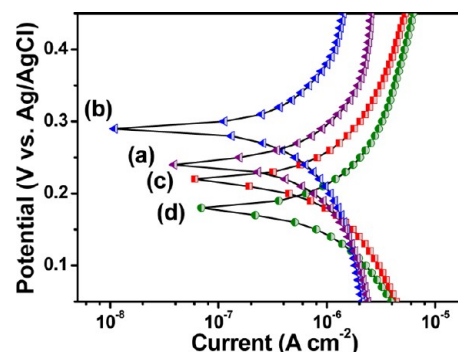
Figure 5. Effect of PPy coating on the corrosion behavior. Representative potentiodynamic polarization curves for (a) Ag-PPy nanoparticles (shell thickness of 13 nm), (b) Ag-PPy nanoparticles (shell thickness of 17 nm), (c) Ag-1, and (d) Ag-2 measured in distilled water, at room temperature, and at 1 mV s^{-1}.

nanoparticles. For comparison, silver nanoparticles enclosed by a thicker PPy shell (17 ± 7 nm) were tested (see Figure S1 in the Supporting Information), as well as the bare silver nanoparticles. Representative Tafel plots from the polarization curves are presented in Figure 5a and the following corrosion parameters derived from curves are summarized in Table 1: E_{corr}, I_{corr}, Tafel slopes b_a and b_c, polarization resistance R_p, and protection efficiency P. Compared with the bare silver nanoparticles, the corrosion potentials of the core−shell nanoparticles shifted to more positive values. In addition, the corrosion current density (I_{corr}) was determined by extrapolating the anodic and cathodic linear portions of the polarization curves to the corrosion potential (E_{corr}). The core−shell nanoparticles showed decreased corrosion current densities that were dependent on the shell thickness. In other words, the corrosion current density decreased with increasing PPy shell thickness. This result strongly implies that the PPy shell played an important role in preventing an electrochemically corrosive mechanism from acting on the silver core. The core−shell nanoparticles showed variations in cathodic and anodic slopes, indicating that the PPy shell affected both cathodic and anodic reactions. During the polarization process, the electrons generated from silver at the anode need to be consumed by a cathodic reaction. The Tafel slope, which is inversely proportional to the electron transfer coefficient and the number of electrons transferred, exhibited a tendency to increase with the PPy coating, suggesting that the PPy shell blocked the electrochemical reactions occurring on the silver surface. The polarization resistance can be used as a quantitative measure of the corrosion resistance because it behaves like a resistor for the polarization of an electrode material. Compared with the control samples, the core−shell nanoparticles exhibited higher polarization resistances, which are indicative of higher corrosion resistances. The percentage protection efficiency can be calculated for the PPy shell from the measured corrosion current densities. Obviously, the protection efficiency of the thicker PPy shell was superior.

Electrochemical corrosion proceeds via two critical reaction processes: (i) the transfer of electrons at the electrode/ electrolyte interface (charge transfer controlled current), and (ii) the movement of reactants or products at distances close to the electrode (mass transport controlled current). To prevent

4360

dx.doi.org/10.1021/am3009967 | ACS Appl. Mater. Interfaces 2012, 4, 4357−4365

Table 1. Major Corrosion Parameters and Calculated Protection Efficiencies for the Ag-PPy Nanoparticles with Different PPy shell Thicknesses and the Control Silver Samples

material	Parameters					
	E_{corr} (mV)	I_{corr} (μA cm^{-2})	b_a	b_c	R_p (kΩ μcm^2)	P (%)
Ag-1	213 ± 3	3.9 ± 0.2	0.63 ± 0.08	0.53 ± 0.04	66 ± 4	
Ag-2	174 ± 3	4.4 ± 0.3	0.68 ± 0.11	0.45 ± 0.03	58 ± 4	
Ag-PPy (13 nm)[a]	247 ± 1	3.2 ± 0.1	0.64 ± 0.02	0.73 ± 0.15	96 ± 6	23.8
Ag-PPy (17 nm)[a]	286 ± 1	2.2 ± 0.1	0.72 ± 0.12	0.61 ± 0.11	147 ± 3	46.9

[a]PPy shell thickness.

corrosion, one or both of these reactions should be limited. The conductivity of the PPy forming the shell is undoubtedly lower than that of the silver core. In addition, the shell thickness can affect the diffusion of electrochemically relevant species into and out of the core. Accordingly, both of the above mechanisms can account for the enhanced anticorrosive behavior of the Ag-PPy nanoparticles. To provide further insight into the anticorrosive activity of the PPy shell, potentiodynamic polarization measurements were performed for four different doping states, as shown in Figure 6. The major corrosion
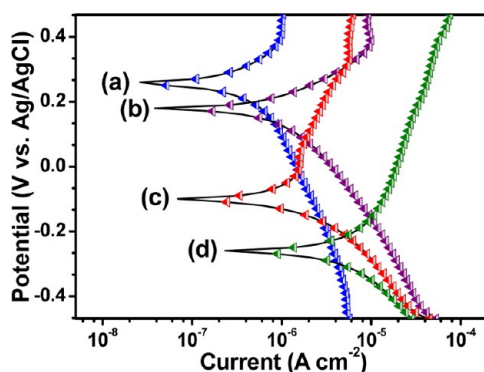
Figure 6. Effect of the doping state of PPy on the corrosion behavior. Representative potentiodynamic polarization curves for silver nanoparticles with (a) neutral, (b) sulfuric acid-, (c) DBSA-, and (d) hydrochloric acid-treated PPy shells measured in distilled water, at room temperature, and at 1 mV s^{-1}.

parameters were derived from these potentiodynamic polarization measurements and are presented in Table 2. First, the dedoped PPy shell exhibited the best protection efficiency. PPy is electrically nonconductive in the dedoped state. Thus, the dedoped PPy shell can preclude charge transfer reactions between the silver and the electrolyte. The Tafel polarization plot for the dedoped PPy shell was asymmetrical, and passive behavior was observed at the anode, suggesting that the PPy layer encasing the silver nanoparticle served as a protective barrier against further corrosion (by sacrificial silver dissolution). In order to examine the effect of counterions, the

dedoped PPy shell was redoped by immersing the core−shell nanoparticles in several acidic solutions. After treatment with dodecylbenzenesulfonic acid (DBSA) and sulfuric acid, the core−shell nanoparticles revealed a slight increase in corrosion current density, although the values continued to be lower than those of the bare silver nanoparticles. The corresponding Tafel plots remained asymmetrically shaped. However, both anodic and cathodic currents were increased by about 1 order of magnitude as compared with those of the dedoped PPy shell. The doping of the counterions into the PPy shell increased the electrical conductivity, which would lead to a slightly enhanced level of charge transfer reactions at the anode and cathode. Interestingly, the treatment of the dedoped PPy shell with hydrochloric acid produced an effect opposite to the above result. After hydrochloric acid treatment, the corrosion current density of the core−shell nanoparticles became higher than even that of the bare silver nanoparticles, indicating that the hydrochloric acid-PPy shell facilitated the corrosion of the silver core. The core−shell nanoparticle electrode may have been undermined upon exposure to hydrochloric acid, in which case a similar increase in both anodic and cathode currents would be expected. However, compared with the cases of DBSA and sulfuric acid, the cathodic current remained relatively unchanged, and instead the anodic current was increased by about 1 order of magnitude. This result is suggestive of some changes in the corrosion system during the anodic polarization. Chloride ions reduce the redox potential of silver species from 0.80 V (Ag$^+$/Ag vs SHE) to 0.22 V (AgCl/Ag).[42] In contrast, the sulfate ion from sulfuric acid has only a small effect on the redox potential of silver species (Ag$_2$SO$_4$/Ag: 0.71 V). Therefore, the presence of chloride ions around the silver core facilitates the oxidation of silver atoms at lower potentials, which is likely the major reason for the adverse effect on the corrosion protection.

The above findings imply that the PPy shell coated on the silver core offers corrosion resistance, the extent of which was strongly dependent on the doping state. In an electrochemically corrosive environment, the surface of the nanoparticles is the most vulnerable. Hence, the surface morphology of the nanoparticles was examined using scanning electron microscopy (SEM) to directly evaluate the protection ability of the

Table 2. Major corrosion Parameters and Calculated Protection Efficiencies for the Ag-PPy Nanoparticles with Different PPy Doping States

| dopant	Parameters					
	E_{corr} (mV)	I_{corr} (μA cm^{-2})	b_a	b_c	R_p (kΩ μcm^2)	P (%)
dedoped	264 ± 4	1.0 ± 0.1	0.46 ± 0.03	0.59 ± 0.07	201 ± 5	75.5
H$_2$SO$_4$	175 ± 3	1.6 ± 0.1	0.32 ± 0.02	0.41 ± 0.04	62 ± 6	61.3
DBSA	−97 ± 2	1.9 ± 0.1	0.72 ± 0.09	0.41 ± 0.05	72 ± 5	53.6
HCl	−264 ± 4	9.2 ± 0.5	0.42 ± 0.03	0.32 ± 0.03	16 ± 3	−120.9

PPy shell. To obtain a clear result, the potentiodynamic polarization experiments were carried out in 1 M sulfuric acid solution for the as-synthesized Ag-PPy nanoparticles and two bare silver nanoparticle samples. Both anodic and cathodic reactions were expected to be facilitated in the sulfuric acid solution. Figure 7 shows typical SEM images of the
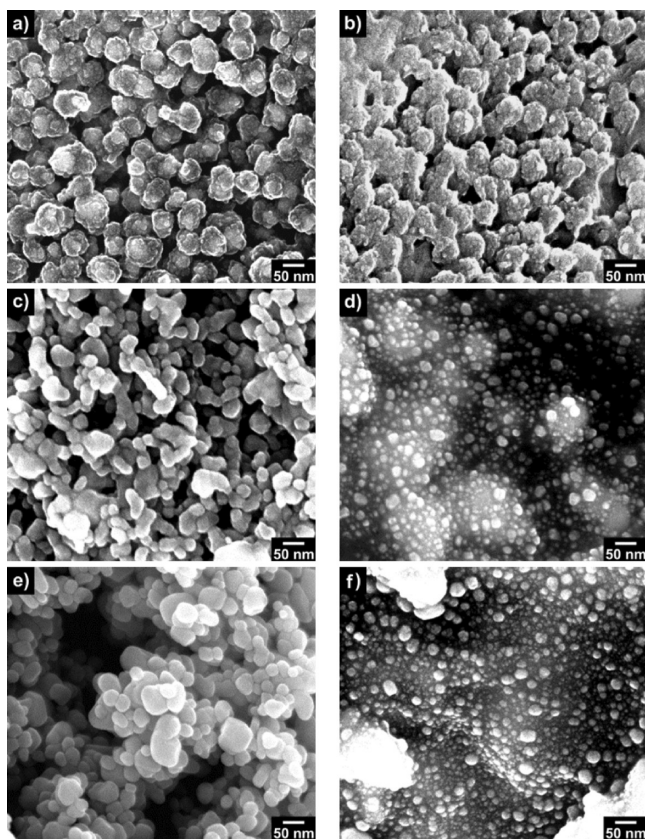
Figure 7. SEM images of the nanoparticle electrodes (a, c, e) before and (b, d, f) after one-cycle potentiodynamic polarization in sulfuric acid solution: (a, b) Ag-PPy, (c, d) Ag-1, and (e, f) Ag-2.

nanoparticles before and after potentiodynamic polarization up to ±500 mV. Surprisingly, however, the Ag-PPy core−shell nanoparticles preserved their morphology after the potentiodynamic polarization, although their surfaces became slightly irregular and rough. In comparison, the anodic dissolution from nanoparticulate silver was more serious than expected. The bare silver nanoparticles were significantly reduced (50 to 80%) in size due to extensive dissolution of silver atoms. This clear difference in the resulting morphology confirmed the effectiveness of the PPy shell in resisting electrochemical corrosion.

Tarnishing of metals is a familiar corrosion phenomenon that is mediated by surface chemical reactions. Silver is apt to be tarnished with sulfur-containing substances as silver sulfide or silver sulfate is formed on the surface. In the case of the Ag-PPy core−shell nanoparticles, however, the unique π-electron conjugated system of PPy provided a chemical barrier, as well as a simple physical barrier, to suppress the tarnishing reaction. Accordingly, the Ag-PPy nanoparticles and bare silver nanoparticles were exposed to sulfur ions in aqueous sodium sulfide solution and their tarnishing behavior was monitored by UV−visible absorption spectroscopy (Figure 8). The silver core reacts with dissolved sulfide species (H_2S or HS^-) in the
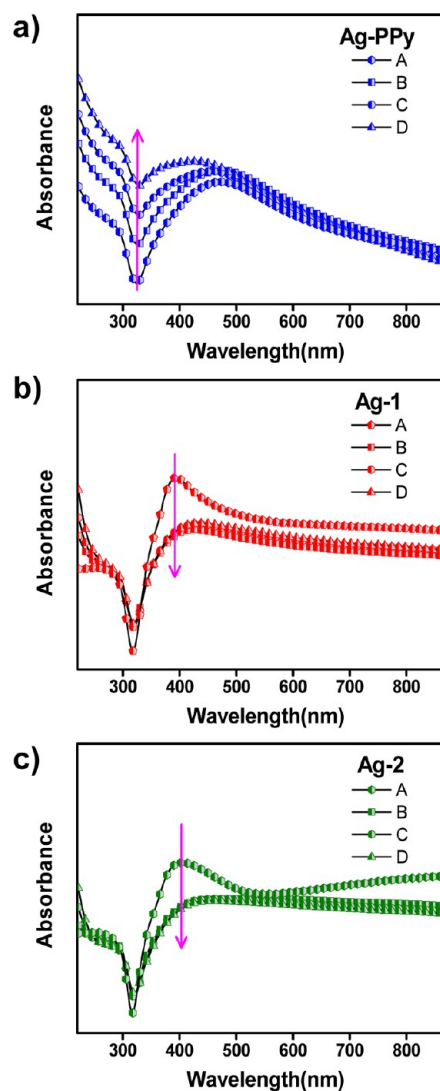

Figure 8. UV−visible absorption spectra of the nanoparticles in aqueous sulfide solution: (a) Ag-PPy, (b) Ag-1, and (c) Ag-2. Arrows indicate the variation of the surface plasmon band with increasing sulfide concentration. ((A) 0.00, (B) 0.25, (C) 0.50, and (D) 0.75 mM).

presence of oxygen to produce silver sulfide,[43] which in turn prohibits the surface plasmon resonance from the silver core. Upon exposure to sulfide ions, as seen in Figure 8, the surface plasmon resonance of the Ag-PPy nanoparticles gradually weakened with increasing sulfide ion concentration. On the other hand, the bare silver nanoparticles lost their surface plasmon characteristic even at the lowest sulfide concentration (0.25 mM). The sulfidation rate of the silver core protected by the PPy shell was slower than that of the bare silver nanoparticles, which implied that the PPy shell can impede tarnishing of the silver core. It can be postulated that the PPy shell physically restricts the diffusion of sulfide ions to the silver core and also holds sulfide ions as counterions in its molecular structure.

To better understand how the nanoparticles are affected by the dissolved sulfur ion, the morphology of the reaction products was examined. For comparison, typical SEM images of the nanoparticles before and after exposure to sulfur ion are presented in Figure 9. Remarkably, the Ag-PPy nanoparticles retained their original morphology after being aged in the
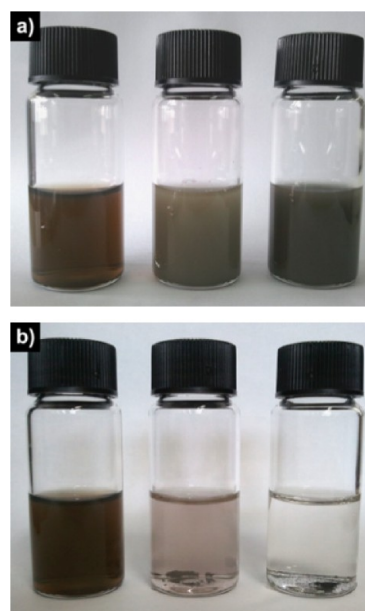
4362

dx.doi.org/10.1021/am3009967 | ACS Appl. Mater. Interfaces 2012, 4, 4357−4365
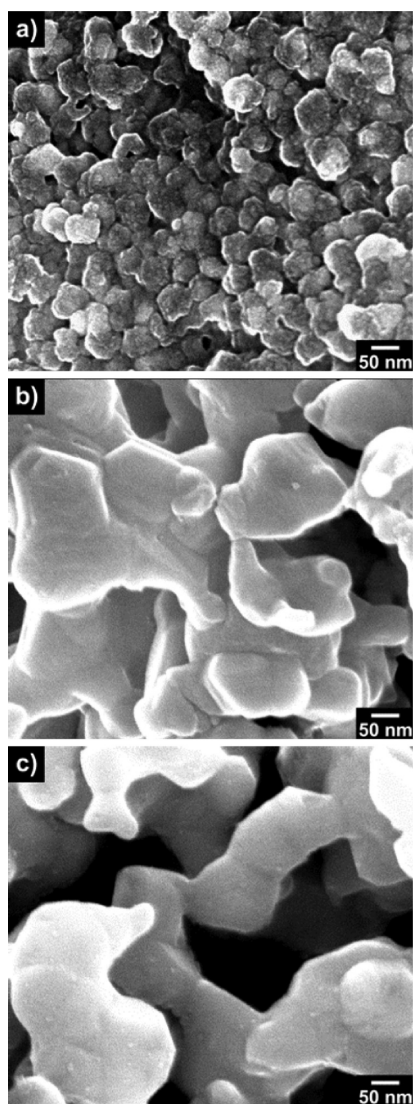
Figure 9. SEM images of the nanoparticles aged in 10 mM aqueous sulfide solution for 10 min.

Figure 10. Photos of the solutions containing the nanoparticles in the (a) absence and (b) presence of 10 mM sulfur ion.

sulfide solution, in stark contrast to the bare silver nanoparticles, which were fused together to form bulky aggregates. A previous report suggested that the surface atoms on the silver nanoparticles are oxidized through reaction with sulfur, partially dissolved, and finally resolidified into Ag_2S to bridge the nanoparticles.[16] Therefore, the tarnishing of silver by sulfur at the nanometer scale is considered to yield its qualitative as well as structural deformation. Colloidal stability, an important physical property for the nanoparticles, was also considerably affected by the tarnishing processing. Figure 10 shows the effect of sulfur tarnishing on nanoparticle colloidal stability. All the nanoparticles were relatively well dispersed in distilled water (Figure 10a). However, upon exposure to 10 mM sulfur ions, their colloidal stability exhibited greatly divergent behavior (Figure 10b). Although bulky precipitates were observed for the bare silver nanoparticles, no precipitates were observed for the Ag-PPy nanoparticles. Compared with the bare silver counterparts, the Ag-PPy nanoparticles tended to be more stable against sulfidation-induced aggregation and subsequent precipitation.

Corrosion and catalysis are similar in sense that both involve surface reactions. In that respect, the catalytic activity of the Ag-

PPy nanoparticles was explored to further understand the function of the PPy shell as the coating layer of the silver core. The reduction of a hazardous pollutant, 4-nitrophenol, with sodium borohydride to a useful compound, 4-aminophenol, was chosen as a model reaction.[44,45] Nitrophenol forms nitrophenolate ion in an aqueous solution of sodium borohydride, and the nitrophenolate ion can be reduced to aminophenolate ion only in the presence of an appropriate catalyst. UV−visible spectrophotometric analysis substantiated that the Ag-PPy nanoparticles served as a catalyst for the reduction reaction. Figure 11a exhibits the time-dependent evolution of the UV−visible spectra of 4-nitrophenol/sodium borohydride reaction mixture containing 0.1 wt % Ag-PPy nanoparticles. The absorption band of the nitrophenolate ions at ca. 400 nm decreased while that at ca. 300 nm increased due to the formation of aminophenolate ions. Since sodium borohydride was used in excess relative to 4-nitrophenol, the rate of catalytic reaction, which is synonymous with the rate of 4-nitrophenol depletion, can be described by the following first-order kinetic equation

$$\frac{d[\mathrm{NP}]}{dt} = -k[\mathrm{NP}]$$

where NP and k designate 4-nitrophenol and the rate constant, respectively. The concentration of 4-nitrophenol is related to the absorbance at 400 nm. Figure 11b exhibits a good linear correlation between $\ln(A_t/A_0)$ and the reaction time, where A_t and A_0 are the time-dependent absorbance and initial absorbance at 400 nm, respectively. Therefore, the rate constant could be determined from the slope of the plot of $\ln(A_t/A_0)$ versus time. The rate constant for the Ag-PPy nanoparticles was 1.1×10^{-3} s^{-1}, which was about 33% less than the average value for the bare silver nanoparticles. The catalytic reaction proceeds when the reactant comes in contact with the silver core. The effective contact of the reactant with the silver surface is basically restricted by the PPy shell, which would lower the catalytic efficiency. Consequently, the PPy shell provides a barrier effect for the chemical reaction, which is
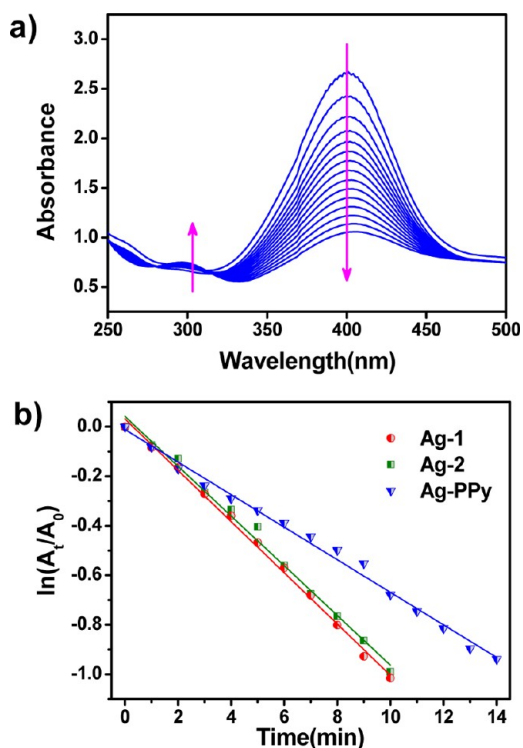
Figure 11. (a) UV–visible absorption spectra during the successive reduction of 4-nitrophenol catalyzed by Ag-PPy nanoparticles at intervals of 1 min. (b) Plots of $\ln(A_t/A_0)$ versus time, where A_t and A_0 note time-dependent absorbance and initial absorbance at 400 nm, respectively, for the reduction of 4-nitrophenol catalyzed by Ag-PPy nanoparticles, Ag-1, and Ag-2.

consistent with the function of the PPy shell as deduced from the corrosion tests.

4. CONCLUSIONS

A conjugated polymer, consisting of a PPy coating on silver nanoparticles, substantially mitigated the corrosion behavior of nanoparticulate silver toward electrochemical corrosion and sulfur tarnishing. The ability of the PPy shell to protect the silver core against electrochemical corrosion depended on the thickness and doping state of the conjugated polymer shell. In addition, the PPy shell enabled the nanoparticles to retain their morphology and colloidal stability under sulfidation. For the reduction reaction of 4-nitrophenol, the Ag-PPy nanoparticles had a lower catalytic efficiency than the bare silver nanoparticles. Since sulfidation is also a chemical reaction, the PPy shell was shown to impede the chemical reactivity of the nanoscale noble metal. We therefore propose that the conjugated polymer coating can provide electrical, chemical, and physical barrier effects for anticorrosion activities under appropriate conditions. The combination of noble metals and conjugated polymers at the nanoscale is of great importance and has valuable potential applications in the areas of microelectronics, sensors and energy devices because of their unique physical and chemical properties. Therefore, the above findings are expected to provide a new insight into materials design for a variety of advanced applications.

■ ASSOCIATED CONTENT

Ⓢ Supporting Information

Additional information associated with the TEM image of Ag nanoparticles encased by a thicker PPy shell and UV–visible spectra recorded during the reduction of 4-nitrophenol. This material is available free of charge via the Internet at http://pubs.acs.org.

■ AUTHOR INFORMATION

Corresponding Author
*E-mail: hyoon@chonnam.ac.kr (H.Y.); ereichmanis@chbe.gatech.edu (E.R.).

Author Contributions
‡These authors equally contributed to this work.

Notes
The authors declare no competing financial interest.

■ ACKNOWLEDGMENTS

■ REFERENCES

(1) Daniel, M. C.; Astruc, D. *Chem. Rev.* **2004**, *104*, 293−346.
(2) Campelo, J. M.; Luna, D.; Luque, R.; Marinas, J. M.; Romero, A. A. *ChemSusChem* **2009**, *2*, 18−45.
(3) Xia, X.; Zeng, J.; Oetjen, L. K.; Li, Q.; Xia, Y. *J. Am. Chem. Soc.* **2012**, *134*, 1793−1801.
(4) Xia, Y.; Li, W.; Cobley, C. M.; Chen, J.; Xia, Z.; Zhang, Q.; Yang, M.; Cho, E. C.; Brown, P. K. *Acc. Chem. Res.* **2011**, *44*, 914−924.
(5) Snow, E. S.; Perkins, F. K.; Houser, E. J.; Badescu, S. C.; Reinecke, T. L. *Science* **2005**, *307*, 1942−1945.
(6) Keren, K.; Berman, R. S.; Buchstab, E.; Sivan, U.; Braun, E. *Science* **2003**, *302*, 1380−1382.
(7) Perelaer, J.; de Gans, B. J.; Schubert, U. S. *Adv. Mater.* **2006**, *18*, 2101−2104.
(8) Li, L.; Ling, Q. D.; Lim, S. L.; Tan, Y. P.; Zhu, C.; Chan, D. S. H.; Kang, E. T.; Neoh, K. G. *Org. Electron.* **2007**, *8*, 401−406.
(9) Krebs, F. C.; Tromholt, T.; Jorgensen, M. *Nanoscale* **2010**, *2*, 873−886.
(10) Hu, L.; Kim, H. S.; Lee, J. Y.; Peumans, P.; Cui, Y. *ACS Nano* **2010**, *4*, 2955−2963.
(11) Nakanishi, H.; Grzybowski, B. A. *J. Phys. Chem. Lett.* **2010**, *1*, 1428−1431.
(12) Christensen, C. H.; Nørskov, J. K. *Science* **2010**, *327*, 278−279.
(13) Narayanan, R.; El-Sayed, M. A. *J. Phys. Chem. B* **2005**, *109*, 12663−12676.
(14) Elechiguerra, J. L.; Larios-Lopez, L.; Liu, C.; Garcia-Gutierrez, D.; Camacho-Bragado, A.; Yacaman, M. J. *Chem. Mater.* **2005**, *17*, 6042−6052.
(15) Mcmahon, M.; Lopez, R.; Meyer, H. M.; Feldman, L. C.; Haglund, R. F. *Appl Phys B-Lasers O* **2005**, *80*, 915−921.
(16) Levard, C.; Reinsch, B. C.; Michel, F. M.; Oumahi, C.; Lowry, G. V.; Brown, G. E. *Environ. Sci. Technol.* **2011**, *45*, 5260−5266.
(17) Prasai, D.; Tuberquia, J. C.; Harl, R. R.; Jennings, G. K.; Bolotin, K. I. *ACS Nano* **2012**, *6*, 1102−1108.
(18) Borisova, D.; Möhwald, H.; Shchukin, D. G. *ACS Nano* **2011**, *5*, 1939−1946.
(19) Skorb, E. V.; Skirtach, A. G.; Sviridov, D. V.; Shchukin, D. G.; Möhwald, H. *ACS Nano* **2009**, *3*, 1753−1760.

(20) Pech, D.; Steyer, P.; Loir, A. S.; Sanchez-Lopez, J. C.; Millet, J. P. *Surf. Coat. Technol.* **2006**, *201*, 347−352.

(21) Combellas, C.; Delamar, M.; Kanoufi, F.; Pinson, J.; Podvorica, F. I. *Chem. Mater.* **2005**, *17*, 3968−3975.

(22) Andion, L. G.; Garces, P.; Lapuente, R.; Vazquez, J. L.; Cases, F. *Corros. Sci.* **2002**, *44*, 2805−2816.

(23) Tallman, D. E.; Spinks, G.; Dominis, A.; Wallace, G. G. *J. Solid State Electrochem.* **2002**, *6*, 73−84.

(24) Spinks, G. M.; Dominis, A. J.; Wallace, G. G.; Tallman, D. E. *J. Solid State Electrochem.* **2002**, *6*, 85−100.

(25) Chen, F.; Liu, P. *ACS Appl. Mater. Interfaces* **2011**, *3*, 2694−2702.

(26) Ishizaki, T.; Masuda, Y.; Sakamoto, M. *Langmuir* **2011**, *27*, 4780−4788.

(27) Li, Z.; Sun, P.; Jing, X. *ACS Appl. Mater. Interfaces* **2011**, *3*, 2694−2702.

(28) Andreeva, D. V.; Skorb, E. V.; Shchukin, D. G. *ACS Appl. Mater. Interfaces* **2010**, *2*, 1954−1962.

(29) Pylypenko, S.; Blizanac, B. B.; Olson, T. S.; Konopka, D.; Atanassov, P. *ACS Appl. Mater. Interfaces* **2009**, *1*, 604−611.

(30) Snihirova, D.; Lamaka, S. V.; Taryba, M.; Salak, A. N.; Kallip, S.; Zheludkevich, M. L.; Ferreira, M. G. S.; Montemor, M. F. *ACS Appl. Mater. Interfaces* **2010**, *2*, 3011−3022.

(31) Fujii, S.; Aichi, A.; Akamatsu, K.; Nawafune, H.; Nakamura, Y. *J. Mater. Chem.* **2007**, *17*, 3777−3779.

(32) Feng, X.; Huang, H.; Ye, Q.; Zhu, J. −J.; Hou, W. *J. Phys. Chem. C* **2007**, *111*, 8463−8468.

(33) Yang, X.; Li, L.; Shang, S.; Pan, G.; Yu, X.; Yan, G. *Mater. Lett.* **2010**, *64*, 1918−1920.

(34) Muňoz-Rojaas, D.; Oró-Solé, J.; Ayyad, O.; Gómez-Romero, P. *Small* **2008**, *4*, 1301−1306.

(35) Chen, A.; Kamata, K.; Nakagawa, M.; Iyoda, T.; Wang, H.; Li, X. *J. Phys. Chem. B* **2005**, *109*, 18283−18288.

(36) Cheng, D.; Xia, H.; Chan, H. S.O. *Langmuir* **2004**, *20*, 9909−9912.

(37) Yang, J.; Yin, H.; Jia, J.; Wei, Y. *Langmuir* **2011**, *27*, 5047−5053.

(38) Chang, M.; Reichmanis, E. *Colloid Polym. Sci.* **2012**, DOI: 10.1007/s00396-012-2731-x.

(39) Chen, A.; Xie, H.; Wang, H.; Li, H.; Li, X. *Synth. Met.* **2006**, *156*, 346−350.

(40) Evanoff, D. D., Jr.; Chumanov, G. *J. Phys. Chem. B* **2004**, *108*, 13957−13962.

(41) Solomon, S. D.; Bahadory, M.; Jeyarajasingam, A. V.; Rutkowsky, S. A.; Boritz, C. *J. Chem. Educ.* **2007**, *84*, 322−325.

(42) Bi, Y.; Ye, J. *Chem. Commun.* **2009**, 6551.

(43) Liu, J.; Pennell, K. G.; Hurt, R. H. *Environ. Sci. Technol.* **2011**, *45*, 7345−7353.

(44) Dotzauer, D. M.; Dai, J.; Sun, L.; Bruening, M. L. *Nano Lett.* **2006**, *6*, 2268−2272.

(45) Wunder, S.; Polzer, F.; Lu, Y.; Mei, Y.; Ballauff, M. *J. Phys. Chem. C* **2010**, *114*, 8814−8820.